HHS Public Access

Author manuscript

Retina. Author manuscript; available in PMC 2020 April 30.

Quantitative OCT angiography features for objective classification and staging of diabetic retinopathy

Minhaj Alam, B.S.[1], **Yue Zhang, M.S.**[2], **Jennifer I. Lim, MD**[3], **R.V.P. Chan, MD**[3], **Min Yang, PhD**[2], and **Xincheng Yao, PhD**[1,3]

[1]Department of Bioengineering, University of Illinois at Chicago, Chicago, IL 60607, USA

[2]Department of Mathematics, Statistics and Computer Sciences, University of Illinois at Chicago, Chicago, IL 60612, USA

[3]Department of Ophthalmology and Visual Sciences, University of Illinois at Chicago, Chicago, IL 60612, USA

Abstract

Purpose: This study aims to characterize quantitative optical-coherence-tomography-angiography (OCTA) features of non-proliferative diabetic-retinopathy (NPDR), and to validate them for computer-aided NPDR staging.

Methods: 120 OCTA images from 60 NPDR (mild, moderate and severe stages) patients and 40 images from 20 control subjects were used for this study conducted in a tertiary, subspecialty, academic practice. Both eyes were photographed and all of the OCTAs were 6 mm × 6 mm macular scans. Six quantitative features, i.e., blood vessel tortuosity (BVT), blood vascular caliber (BVC), vessel perimeter index (VPI), blood vessel density (BVD), foveal avascular zone (FAZ) area (FAZ-A), and FAZ contour irregularity (FAZ-CI) were derived from each OCTA image. A support vector machine (SVM) classification model was trained and tested for computer-aided classification of NPDR stages. Sensitivity, specificity and accuracy were used as performance-metrics of computer-aided classification and receiver-operation-characteristics (ROC) curve was plotted to measure the sensitivity-specificity tradeoff of the classification algorithm.

Results: Among six individual OCTA features, BVD shows the best classification accuracies, 93.89% and 90.89% for control vs. disease and control vs. mild-NPDR, respectively. Combined-feature classification achieved improved accuracies, 94.41% and 92.96% respectively. Moreover, the temporal-perifoveal region was the most-sensitive region for early detection of DR. For multi-class classification, SVM algorithm achieved 84% accuracy.

Corresponding author: Xincheng Yao, PhD, Richard & Loan Hill Professor, Department of Bioengineering (MC 563), Professor, Department of Ophthalmology & Visual Sciences, University of Illinois at Chicago (UIC), Clinical Sciences North, Suite W103, Room 164D, 820 South Wood Street, Chicago, IL 60612, Tel: (312)413-2016; Fax: (312)996-4644, xcy@uic.edu.

Conflict of Interest:
No conflicting relationship exists for any author.

Declaration:
The work was completed at the University of Illinois at Chicago.

Conclusion: BVD was observed as the most-sensitive feature and temporal-perifoveal region was the most-sensitive region for early detection of DR. Quantitative OCTA analysis enabled computer-aided identification and staging of NPDR.

Summary Statement:

Quantitative OCTA features are used for computer-aided classification and objective staging of diabetic retinopathy. Blood-vessel density is the most sensitive OCTA feature, and temporal-perifoveal retina is the most sensitive region for detecting early onset of NPDR.

Keywords

Computer-aided diagnosis; Diabetic retinopathy; Medical imaging; Ophthalmology; Optical coherence tomography; Optical diagnostics for medicine; Physiology; Vision system - noninvasive assessment

---

As the major ocular manifestation of diabetes [–], diabetic retinopathy (DR) is a leading cause of preventable blindness worldwide . DR can trigger retinal blood vessels to leak blood and fluids to produce pathological features such as micro-aneurysms, exudates, venous beading, cotton wool spots, etc.. Retinal nonperfusion, hemorrhages and other microvascular abnormalities worsen as DR severity progresses. Currently, diabetes affects 1 in every 11 adults or roughly 415 million people worldwide . As nearly 40–45% patients with diabetes are prone to vision impairment due to DR , early detection and prompt treatment of DR are essential to decrease the progression of vision loss associated with DR. Telemedicine approaches can help ease disparities of care as it allows those in underserved areas to be screened. However, mass-screening programs still heavily depend on experienced ophthalmologists to assess retinal photographs . This process is both time consuming and expensive . An computer-aided diagnostic tool could aid in DR screening and have genuine impact on clinical workflow.

For computer-aided diagnosis of microvascular diseases like DR, researchers in prior work have mostly used fundus photography and spectral-domain optical coherence tomography (SD-OCT) [–], which provide important qualitative information about retinal pathology. However, fundus or SD-OCT images cannot provide quantitative representation of microvascular architecture of the retina . Fluorescein angiography (FA) has been used to evaluate vasculature features of DR [,]. FA requires intravenous dye injections which require involvement of trained professionals. On the contrary, OCT angiography (OCTA) allows depth-resolved visualization of multiple layers in retina with high resolution and may be more sensitive than traditional FA in detecting microvascular changes in retinal diseases . It has been recently used to demonstrate quantitative assessment of retinal vasculature in retinovascular and degenerative retinal conditions.[–].

In a recent study on sickle cell retinopathy patients, our group conducted a comprehensive analysis of OCTA images and demonstrated six quantitative OCTA biomarkers, including blood vessel tortuosity (BVT), blood vascular caliber (BVC), vessel perimeter index (VPI), blood vessel density (BVD), foveal avascular zone (FAZ) area (FAZ-A), and FAZ contour irregularity (FAZ-CI). We also used these six features for computer-aided classification and

staging of SCR patients with three different classification models. It was observed that combined-features show the best accuracy for identifying SCR stages with a support vector machine (SVM) classifier model. In this current study, we refine and extend these established features for computer-aided classification of non-proliferative DR (NPDR). The algorithm measures the six OCTA features of control and disease (mild, moderate and severe NPDR) subjects and inputs them into an SVM model. The SVM classifier trains itself with the compiled features and provides a final diagnostic prediction. We conducted a control vs. disease (NPDR) binary-class classification to identify OCTA images of NPDR patients. We also conducted a multi-class classification to separately classify control and three NPDR stages (mild, moderate and severe) from each other. The classification performance was quantitatively validated using sensitivity, specificity and accuracy metrics along with graphical metrics, i.e., receiver operation characteristics (ROC) curve.

Methods

This section describes our methodology for computer-aided classification of NPDR stages. Figure 1 illustrates the core steps of our algorithm. The first step requires image data processing and the second step machine learning. Image data processing involves data acquisition, pre-processing, feature extraction and compilation for the classification model. Machine learning involves training the classifier model based on the feature set and testing it with cross validation to obtain a final output of a diagnostic prediction.

OCTA image acquisition

This study was approved by the Institutional Review Board of the University of Illinois at Chicago and was in compliance with the ethical standards stated in the Declaration of Helsinki. The DR patients were recruited from University of Illinois at Chicago (UIC) Retinal Clinic. We performed a retrospective study of consecutive diabetic patients (type II) who underwent OCTA and OCT imaging. The patients are thus representative of a university population of diabetic patients who require imaging for management of diabetic macular edema and DR. OCT/OCTA images of both eyes of every patient were collected. We excluded subjects with macular edema, previous vitreous surgery, and history of other eye diseases. Control OCTAs were obtained from healthy volunteers who agreed to undergo OCTA and OCT imaging. All patients had undergone a complete anterior and dilated posterior segment examination (JIL, RVPC). The patients were classified by severity of DR (mild, moderate, severe) according to the Early Treatment Diabetic Retinopathy Study (ETDRS) staging system. The grading was done by retina specialist using a slit lamp fundus lens, technicians did not contribute to the grading of the patients. Fig. 2 illustrates representative OCTA images of superficial and deep layers for control and NPDR eyes and the corresponding OCT B-scan.

SD-OCT data were acquired using an ANGIOVUE SD-OCT angiography system (Optovue, Fremont, CA, USA), with a 70-KHz A-scan rate, an axial resolution of ~5 μm and a lateral resolution of ~15 μm. All the OCTA images were macular scans and had field of view (FOV) of 6 mm × 6 mm. We exported the OCT angiography images from the software ReVue (Optovue, Fremont, CA, USA) and used custom-developed MATLAB (Mathworks,

Natick, MA, USA.) procedures with graphical user interface (GUI) for further image analysis, feature extraction and image classification.

Pre-processing of OCTA images

OCTA images with a 6 mm × 6 mm field of view (304×304 pixels) were used for extracting all vascular and foveal features. To account for light and contrast image variation, we performed multiple preprocessing steps for image standardization before feature extraction and classification. We normalized all the OCTA images to a standard window level based on maximum and minimum intensity values. These preprocessing steps aim to improve the overall reliability of the extracted features and improve the performance of classifier model to identify OCTAs of different stages of NPDR.

Feature extraction

For the computer-aided classification of NPDR stages, six quantitative features were extracted from each OCTA image: BVT, BVC, VPI, BVD, FAZ-A and FAZ-CI. Fig. 1B provides an overview of the processes involved in extracting features and Fig. 3 illustrates the representative images of feature extraction. The rationale of each of these six OCTA features and detailed procedure for measuring them are described in our recent publication . For improved diagnostic accuracy, the segmented FAZ area is excluded when measuring BVD. The segmented FAZ area had 98.43% similarity with manually segmented ground truths.

Statistical analyses

All the statistical analyses were conducted using MATLAB (Mathworks, Natick, MA, USA) and OriginPro (OriginLab Corporation, MA, USA). All the quantitative features for different groups were tested for normality using a Shapiro-Wilk test. For normally distributed variables, one way, multi-label analysis of variance (ANOVA) was used to compare difference of mean values of the features among multiple groups. One versus one comparisons of the features between the control and NPDR stages were performed using Student's t-test. For features that were not normally distributed, we employed non-parametric Kruskal-Wallis test for comparing multiple groups and independent sample t-test (Mann-Whitney) for one versus one comparisons. We used Chi-square test to compare the sex and hypertension distribution among different groups. Age distribution was compared with ANOVA. Spearman's correlation coefficients (r_s) were also calculated to analyze the relationship among the OCTA features and their correlation with DR severity. For all the comparisons, statistical significance was defined with a P value < 0.05. However, the P value was Bonferroni-corrected for multiple simultaneous group comparisons.

Classification model

A SVM classifier was adopted for computer-aided identification of NPDR stages. We separated the classification process into two segmentations. First, we conducted control vs. disease classification (1 vs. 1, binary classification). We used an SVM model to identify disease and control groups. Second, we extended our classification to control vs mild NPDR

to test if our model could identify the mild stage which is the onset of DR that is currently challenging to diagnose in clinical screening.

In the second segment, we conducted a multi-class SVM classification where the classifier model identified control and 3 stages of NPDR from the database. The classification model was trained based on the feature compilation of all the OCTA data and produced a final predicative diagnosis on the test set. For both the binary and multi-class classification, we used a 5-fold cross validation technique to control overfitting [–] and also implemented multiple runs with image data splits to confirm the robustness and repeatability of the computer-aided classification [,,].

The classification algorithm was implemented in MATLAB hosted in a 4-core desktop computer with a Windows-7 64-bit operating system, Core i7–4770 CPU at 3.4 GHz (Intel, Santa Clara, CA, USA), and 16 GB of RAM. For binary classification with SVM model, we employed a one versus one class decision model []. For the multi-class classification, a custom coded SVM function was used in MATLAB which allows prediction of multiple classes with SVM model. The average time for processing a single OCTA image and extracting the feature vectors was ~ 5 seconds. The whole classification process for binary and multi-class prediction took ~ 3–5 seconds and ~ 8–10 seconds, respectively.

The performance of the SVM prediction model for control vs. disease and control vs. mild NPDR was assessed by calculating three comparison metrics, i.e. sensitivity, specificity, and accuracy.[] For multi-class classification, overall accuracy and error rate was measured to evaluate the classification performance. Sensitivity and specificity show the ratio of the cases correctly identified by the classifiers. Accuracy metric was also measured which gives balanced and comprehensive representation of classification performance.

ROC (Receiver Operation Characteristics) curve, a graphical method, was used to evaluate SVM models' prediction performance. In ROC curve, true positive rate (i.e., sensitivity) is plotted as a function of false positive rate (i.e., 1-specificity) at different tradeoff points. AUC (Area under curve) is the area under ROC curve, which is measured to quantify how well the classifier is able to identify the different classes. The closer the curve to the left up corner, the more accuracy the prediction is. AUC equals 1 or 100% represents a perfect prediction, and 0.5 or 50% represents a bad prediction. For all statistical tests used in the study, the significance was considered at $P < 0.05$.

Results

Our OCTA image database consisted of 120 OCTA images from 60 NPDR patients and 40 images from 20 control subjects. We originally had 65 sets of NPDR patient data and 20 sets of control subjects' data, but we had to exclude 6 eyes due to poor OCTA acquisition and another 4 eyes as they had presence of other retinal diseases. Among the NPDR OCTAs, we had 20 sets of mild, moderate and severe stage data (40 OCTAs for each stage). The detailed patient demographic data are shown in table 1. There was no statistical significance in the distribution of age, sex and hypertension between control and DR groups. (ANOVA, $P = 0.14$; chi-square test, $P = 0.11$ and $P = 0.32$, respectively).

Quantitative OCTA features

All the quantitative features except BVT and FAZ-A were normally distributed (Shapiro-Wilk test, P > 0.05). BVT and FAZ-A had slightly right-skewed distributions and marginal P values (0.046 and 0.048 respectively). A summary of the quantitative features used for control and NPDR OCTA image analysis is shown in Table 2. We observe increase in BVT, BVC, FAZ-A and FAZ-CI with progression of NPDR severity. On the other hand, BVD and VPI progressively decreased with NPDR severity. In case of control vs. NPDR, the difference in all the OCTA features were statistically significant (Student t-test for BVC, VPI, BVD and FAZ-CI, P < 0.008, P < 0.005 and P < 0.001 for control vs. mild, moderate and severe NPDR, respectively; Independent sample t-test (Mann-Whitney) for BVT and FAZ-A, P < 0.008, P < 0.008 and P < 0.005 for control vs. mild, moderate and severe NPDR, respectively). However, when comparing features among NPDR groups, not all features show significant differences. BVT and BVC were not statistically significant considering Bonferroni-corrected P value (Kruskal-Wallis, P = 0.044 and ANOVA, P = 0.038). However, the changes in BVD, VPI, FAZ-CI and FAZ-A were statistically significant (ANOVA, P = 0.001, 0.006, 0.004 respectively and Kruskal-Wallis, P = 0.006).

Spearman's rank test was performed to analyze the relationship among the OCTA features and their correlation with NPDR severity. BVD and VPI showed negative correlation, while BVT, BVC, FAZ-A and FAZ-CI showed positive correlation with NPDR stages (r_s = −0.512, −0.633, +0.438, +0.451, +0.549, +0.537 respectively; all P < 0.002). In the parafoveal area of the superficial layer, BVT showed significant negative correlation with FAZ-A and FAZ-CI (r_s = −0.237, −0.241 and P = 0.007, 0.006 respectively in moderate and severe stage NPDR). Perifoveal BVD (superficial layer) also showed significant negative correlation with FAZ-A and FAZ-CI (r_s = −0.211, −0.318 respectively and P < 0.008 for both in moderate and severe stage NPDR). In both superficial and deep layers, FAZ-A and FAZ-CI showed statistically significant positive correlation in severe stage NPDR (r_s = −0.196, −0. 204 and P < 0.008). BVD and VPI also showed strong positive correlation in the perifoveal retina (superficial layer) for severe stage NPDR (r_s = −0.228, and P < 0.006).

Classification: Control vs. disease and control vs. mild NPDR

Figure 4A and Fig. 4B show mean ROC curves to illustrate the performance of the SVM classifier for control vs. disease and control vs. mild NPDR classifications, respectively. The area under the ROC curve was measured to quantify how well the classifier was able to identify the different classes. ·. We observed 92.33% and 91.98% AUCs in control vs. disease and control vs. mild NPDR classifications using combined features. The > 90% AUC in both cases establishes the ability of the SVM model to identify NPDR from control subjects. Table 3 provides detailed comparison in terms of sensitivity, specificity and accuracy along with AUC (the highest percentage possible is 100%) . In table 3, FAZ-A, FAZ-CI and BVD provide reasonable accuracy and AUC (>90% for both control vs. disease and control vs. mild NPDR). By combining all six features together, enhanced classification performance, i.e., 95.17% sensitivity, 93.88% specificity and 94.41% accuracy in control vs. disease classification and 94.45% sensitivity, 92.29% specificity and 92.96% accuracy in control vs. mild NPDR classification, was observed.

Most sensitive OCTA feature and retinal region

We observed that BVD provides the best classification sensitivity as a single feature (accuracy 93.89% for control vs. disease and 92.75% for control vs. mild NPDR) (Table 3). Further analysis of the BVD feature in localized areas (Fig. 5A) is summarized in table 4. Compared to parafoveal BVD (80.65% for control vs. disease and 76.22% control vs. mild NPDR), the perifoveal region shows better sensitivity (90.77% for control vs. disease and 89.64% control vs. mild NPDR) (Fig. 5B). We further divided the perifoveal region into four regions based on their orientation: nasal, superior, temporal and inferior region (Fig. 5C and table 5). BVD measured from the temporal region of the perifoveal zone is the most sensitive to predict onset of mild NPDR.

Multi-class classification

We also conducted a multi-class classification to classify control and NPDR stages for assessing predictive diagnosis. The SVM predictor model trained and tested on the whole database provided overall accuracy of 83.94% (Control or NPDR stages) with classifying error of 16.06%.

Discussion

In the study, we demonstrate an automated algorithm for computer-aided classification of NPDR with six quantitative OCTA features, including BVT, BVC, VPI, BVD, FAZ-A and FAZ-CI. OCTA images provide proper visualization of microvascular architecture in intraretinal layers which permits a comprehensive quantitative analysis of pathological changes due to retinal diseases (i.e. NPDR) and their progression. In our previous work, we have conducted a comprehensive analysis of OCTA images of SCR patients and established these six parameters as potential OCTA biomarkers. We also validated computer-aided classification of SCR stages using an SVM classifier model with these six features and obtained 97% accuracy for identifying stage II and III SCR patients. In the current study, we have adapted the strategy for DR OCTA images. This study illustrates the importance of quantitative analysis alongside qualitative observation in DR staging. Morphological changes like impaired capillary perfusion, overall changes in vessel and foveal size and complexity etc. were quantitatively compared and used for staging NPDR severity. We conducted a control vs. NPDR classification and the SVM model identified diseased patients with an accuracy of 94.41%. The SVM classifier model could identify 94.45% control subjects correctly, and detect early NPDR with 92.29% accuracy. Our SVM model established inter-stage OCTA classification of NPDR with a true prediction rate of 83.94%. A proper implementation of this algorithm would facilitate a quick and efficient way of DR screening and diagnosis.

For a comprehensive and robust OCTA classification model, two most important factors are the objectivity of the input features and their sensitivity towards the specific disease, which is DR for this study. We conducted a Pearson’s correlation analysis on the six quantitative parameters and observed low correlation metric among them except for BVD and VPI when compared in 6 mm FOV (excluding FAZ). BVD reflects overall density changes in the retina and VPI reflects vessel perimeter changes. Although they show positive correlation when

compared in whole retina, the correlation is significantly low when compared in different areas specifically (parafoveal, perifoveal or nasal, superior, temporal, inferior). This suggests that the six parameters might reflect different morphological aspects of the diseased retina. Therefore, the parameters are objective and combining them together yielded better classification performance.

In our recent study with SCR OCTAs, we observed that FAZ-A and FAZ-CI were the most sensitive parameters to identify stage II and III SCR. In contrast, for DR patients, the most sensitive parameter is BVD (table 2 and 3). Previous studies of DR OCTAs also confirm statistical significance of density and fractal dimension changes in retinal vasculature[,,]. When comparing BVD in different NPDR groups, we observed statistically significant reduction in BVD with disease progression (Table 3). We observed higher sensitivity of vessel dropout, i.e., BVD reduction, in the perifoveal area (diameter 3–6 mm) compared to parafoveal area (diameter <3 mm). Comparatively lower sensitivity of BVD in the parafoveal area could possibly be attributed to the variable shapes and size of fovea within 3 mm field of view. We further checked the perifoveal area and conducted BVD analysis in four orientations (nasal, superior, temporal and inferior). The temporal and superior regions showed comparatively higher sensitivity. Using BVD feature from these regions, we could classify mild NPDR OCTAs with an accuracy of ~88%. If we consider the whole perifoveal area, the accuracy was ~ 90%. These results suggest that for early onset of DR, it could be important to test BVD in perifoveal retina and more specifically in the temporal region. This reflects the watershed zone of the retinal vasculature.

For implementing any computer-aided screening and diagnostic applications, a big challenge is the computation time needed for overall feature extraction, compilation, classifier modeling and testing. For our demonstrated algorithm, it takes ~ 5 seconds to extract all the features from single OCTA image, 3–5 seconds for both control vs. disease and control vs. mild NPDR classification, and ~ 8–10 seconds for the multi-class classification. For clinical implementation of the computer-aided classification, further optimization may consider inclusion of patient history including duration of diabetes. By controlling the overall variance of these sub-features and adding more optimized quantifying features, overall accuracy of the classification process could be further increased.

Our study had a few limitations. Our sample size was modest for each cohort and all the OCTA data were acquired from one device (Angioview, split-spectrum amplitude decorrelation angiography reconstruction algorithm) in a single location. For future study, we plan to expand the population and to include OCTA data from different devices (e.g. Cirrus Angioplex, Optical micro-angiography reconstruction algorithm) and locations to test the robustness of the computer-aided classification algorithm for identifying NPDR stages. Some other limitations were the potential motion and projection artifacts and segmentation errors of the reconstruction algorithm. We attempted to minimize the effect of these artifacts in our analysis by excluding the images with severe artifacts and patients with macular edema.

In conclusion, quantitative OCTA features enabled objective identification and staging of NPDR with excellent diagnostic accuracy and predictability of DR stages. BVD in temporal

perifoveal region shows the best sensitivity to early DR. Combined-features, i.e., inputting all quantitative OCTA features together, demonstrate enhanced classification accuracy.

Acknowledgement:

The authors thank Mr. Mark Janowicz and Ms. Andrea Degillio (Eye and Ear Infirmary, University of Illinois at Chicago) for technical support of data acquisition.

Financial support: This research was supported in part by NIH grants R01 EY023522, R01 EY024628, P30 EY001792; by unrestricted grant from Research to Prevent Blindness; by Richard and Loan Hill endowment; by Marion H. Schenk Chair endowment.

References

1. Stanga PE, Boyd SR, Hamilton AM. Ocular manifestations of diabetes mellitus. Curr Opin Ophthalmol 1999;10:483–9. [PubMed: 10662255]
2. Akil H, Bulus AD, Andiran N, Alp MN. Ocular manifestations of Type 1 diabetes mellitus in pediatric population. Indian J Ophthalmol 2016;64:654–658. [PubMed: 27853013]
3. Milkie GM. Ocular manifestations associated with diabetes mellitus; a case report. Am J Optom Arch Am Acad Optom 1956;33:604–8. [PubMed: 13372739]
4. Saclarides TJ. Diabetes mellitus: classification, etiology, diagnosis, complications, and possible ocular manifestations. J Ophthalmic Nurs Technol 1982;1:33–9, 50. [PubMed: 6922937]
5. Wilkinson CP, Ferris FL, Klein RE, et al. Proposed international clinical diabetic retinopathy and diabetic macular edema disease severity scales. Ophthalmology 2003;110:1677–1682. [PubMed: 13129861]
6. Nayak J, Bhat PS, Acharya UR, Lim CM, Kagathi M. Automated identification of diabetic retinopathy stages using digital fundus images. J Med Syst 2008;32:107–115. [PubMed: 18461814]
7. International Diabetes Federation (IDF). IDF Diabetes Atlas 7th edition; 2015 http://www.diabetesatlas.org/. Accessed October 20, 2016.
8. Beagley J, Guariguata L, Weil C, Motala AA. Global estimates of undiagnosed diabetes in adults. Diabetes Res Clin Pract 2014;103:150–60. [PubMed: 24300018]
9. Ozieh MN, Bishu KG, Dismuke CE, Egede LE. Trends in health care expenditure in U.S. adults with diabetes: 2002–2011. Diabetes Care 2015;38:1844–51. [PubMed: 26203060]
10. Shah SAA, Laude A, Faye I, Tang TB. Automated microaneurysm detection in diabetic retinopathy using curvelet transform. Journal of Biomedical Optics 2016;21.
11. Goh JK, Cheung CY, Sim SS, Tan PC, Tan GS, Wong TY. Retinal Imaging Techniques for Diabetic Retinopathy Screening. J Diabetes Sci Technol 2016;10:282–94. [PubMed: 26830491]
12. Mookiah MR, Acharya UR, Chua CK, Lim CM, Ng EY, Laude A. Computer-aided diagnosis of diabetic retinopathy: a review. Comput Biol Med 2013;43:2136–55. [PubMed: 24290931]
13. Winder RJ, Morrow PJ, McRitchie IN, Bailie JR, Hart PM. Algorithms for digital image processing in diabetic retinopathy. Comput Med Imaging Graph 2009;33:608–22. [PubMed: 19616920]
14. Virgili G, Menchini F, Murro V, Peluso E, Rosa F, Casazza G. Optical coherence tomography (OCT) for detection of macular oedema in patients with diabetic retinopathy. 2011.
15. Zahid S, Dolz-Marco R, Freund KB, et al. Fractal Dimensional Analysis of Optical Coherence Tomography Angiography in Eyes With Diabetic Retinopathy. Invest Ophth Vis Sci 2016;57:4940–4947.
16. Gass JD. A fluorescein angiographic study of macular dysfunction secondary to retinal vascular disease. VI. X-ray irradiation, carotid artery occlusion, collagen vascular disease, and vitritis. Arch Ophthalmol 1968;80:606–17. [PubMed: 5684309]
17. Talu S, Calugaru DM, Lapascu CA. Characterisation of human non-proliferative diabetic retinopathy using the fractal analysis. Int J Ophthalmol-Chi 2015;8:770–776.

18. Minvielle W, Caillaux V, Cohen SY, et al. Macular Microangiopathy in Sickle Cell Disease Using Optical Coherence Tomography. Angiography. Am J Ophthalmol 2016;164:137–144. [PubMed: 26748057]
19. Lim JI. Ophthalmic manifestations of sickle cell disease: update of the latest findings. Curr Opin Ophthalmol 2012;23:533–536. [PubMed: 23047170]
20. Hoang QV, Chau FY, Shahidi M, Lim JI. Central macular splaying and outer retinal thinning in asymptomatic sickle cell patients by spectral-domain optical coherence tomography. Am J Ophthalmol 2011;151:990–994 e1. [PubMed: 21457923]
21. Asdourian GK, Nagpal KC, Busse B, et al. Macular and perimacular vascular remodelling sickling haemoglobinopathies. Br J Ophthalmol 1976;60:431–53. [PubMed: 952816]
22. Condon PI, Serjeant GR. Ocular Findings in Homozygous Sickle-Cell Anemia in Jamaica. Am J Ophthalmol 1972;73:533–543. [PubMed: 5020172]
23. Ishibazawa A, Nagaoka T, Takahashi A, et al. Optical Coherence Tomography Angiography in Diabetic Retinopathy: A Prospective Pilot Study. Am J Ophthalmol 2015;160:35–44. [PubMed: 25896459]
24. Alam M, Thapa D, Lim JI, Cao D, Yao X. Quantitative characteristics of sickle cell retinopathy in optical coherence tomography angiography. Biomedical Optics Express 2017;8:1741–1753. [PubMed: 28663862]
25. Alam M, Thapa D, Lim JI, Cao D, Yao X. Computer-aided classification of sickle cell retinopathy using quantitative features in optical coherence tomography angiography. Biomedical optics express 2017;8:4206–4216. [PubMed: 28966859]
26. Hastie T, Tibshirani R, Friedman J. Overview of supervised learning The elements of statistical learning: Springer, 2009:9–41.
27. Breiman L, Spector P. Submodel selection and evaluation in regression. The X-random case. International statistical review/revue internationale de Statistique 1992:291–319.
28. James G, Witten D, Hastie T, Tibshirani R. An introduction to statistical learning: Springer, 2013.
29. Kohavi R A study of cross-validation and bootstrap for accuracy estimation and model selection. Ijcai, 1995:1137–1145.
30. Allwein EL, Schapire RE, Singer Y. Reducing multiclass to binary: A unifying approach for margin classifiers. J Mach Learn Res 2000;1:113–141.
31. Escalera S, Pujol O, Radeva P. On the decoding process in ternary error-correcting output codes. Ieee T Pattern Anal 2010;32:120–134.
32. Van Stralen KJ, Stel VS, Reitsma JB, Dekker FW, Zoccali C, Jager KJ. Diagnostic methods I: sensitivity, specificity, and other measures of accuracy. Kidney international 2009;75:1257–1263. [PubMed: 19340091]
33. Baratloo A, Hosseini M, Negida A, El Ashal G. Part 1: simple definition and calculation of accuracy, sensitivity and specificity. 2015.
34. Hajian-Tilaki K Receiver Operating Characteristic (ROC) Curve Analysis for Medical Diagnostic Test Evaluation. Caspian J Intern Med 2013;4:627–35. [PubMed: 24009950]
35. DeLong ER, DeLong DM, Clarke-Pearson DL. Comparing the Areas under Two or More Correlated Receiver Operating Characteristic Curves: A Nonparametric Approach. Biometrics 1988;44:837–845. [PubMed: 3203132]
36. Zhu W, Zeng N, Wang N. Sensitivity, specificity, accuracy, associated confidence interval and ROC analysis with practical SAS implementations. NESUG proceedings: health care and life sciences, Baltimore, Maryland 2010;19.
37. Kim AY, Chu Z, Shahidzadeh A, Wang RK, Puliafito CA, Kashani AH. Quantifying Microvascular Density and Morphology in Diabetic Retinopathy Using Spectral-Domain Optical Coherence Tomography Angiography. Invest Ophthalmol Vis Sci 2016;57:OCT362–70.
38. Lee H, Lee M, Chung H, Kim HC. Quantification of Retinal Vessel Tortuosity in Diabetic Retinopathy Using Optical Coherence Tomography Angiography. Retina 2017.

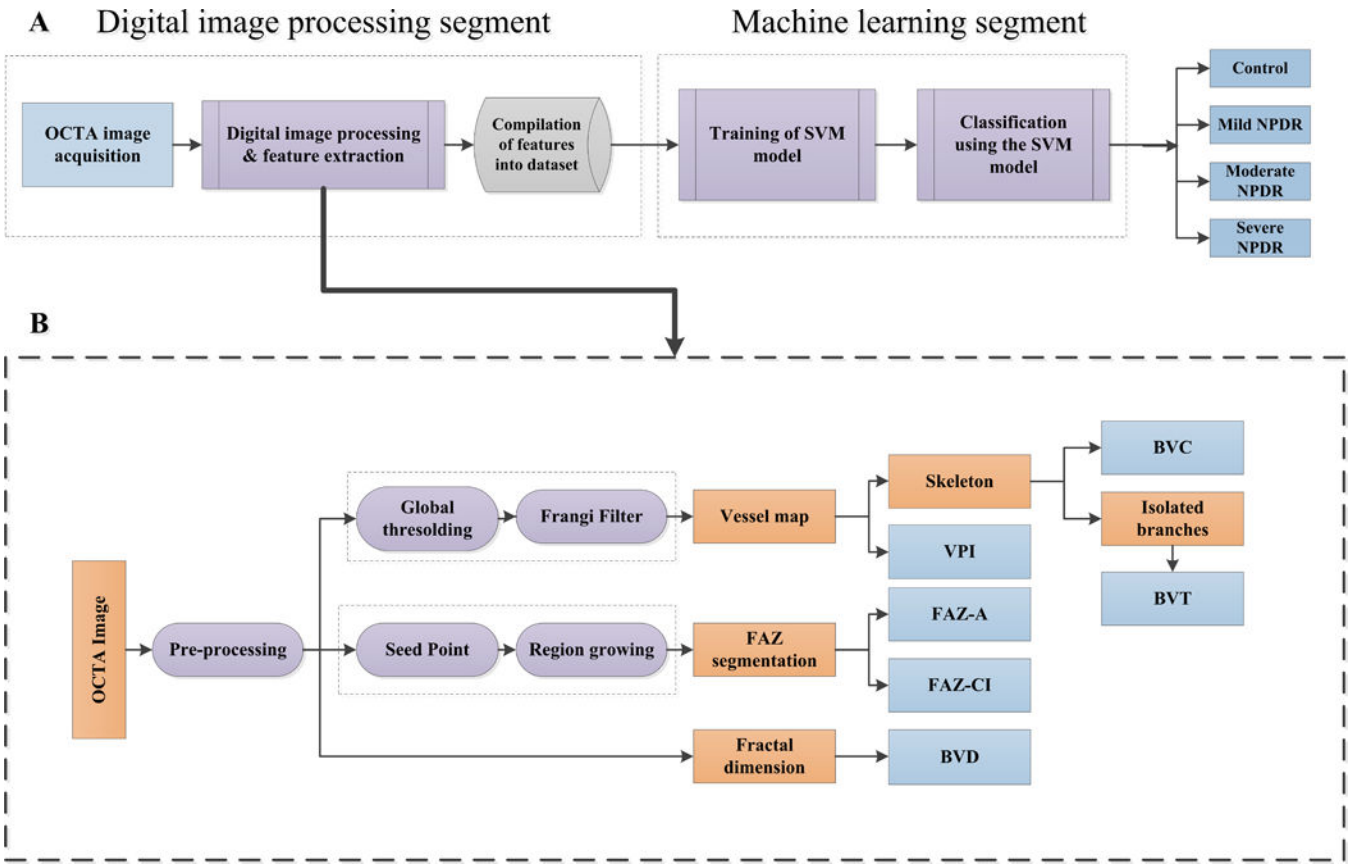

Figure 1.

Illustrating the methodology of proposed algorithm. (A) Diagnostic flowchart of the procedure of computer-aided classification. (B) Detailed feature extraction process.

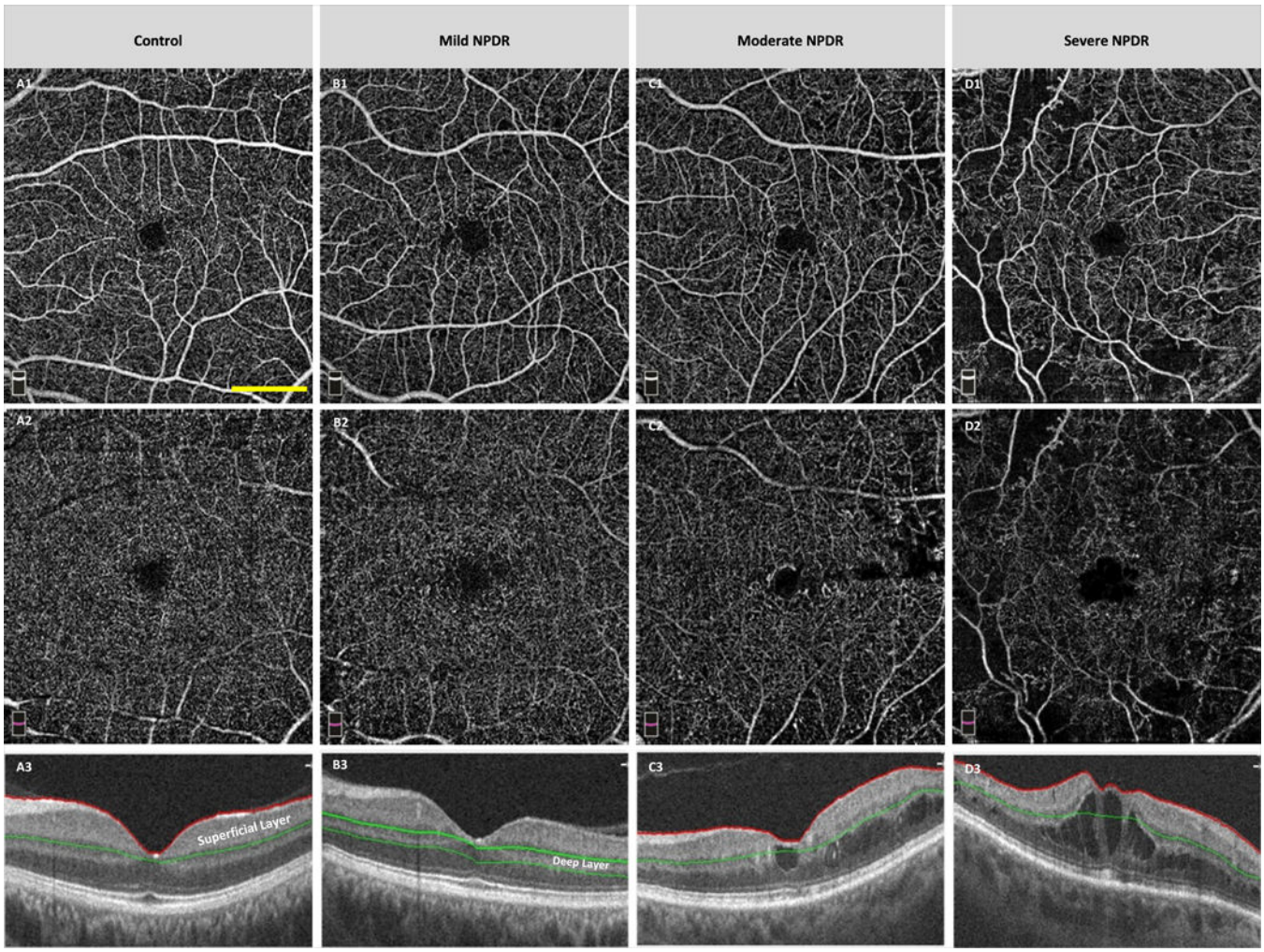

Figure 2.

Representative OCTA images of control (A), mild NPDR (B), moderate NPDR (C), and severe NPDR. The first row (A1, B1, C1, D1) and second row (A2, B2, C2, D2) represent OCTAs from superficial and deep layers respectively. The third row (A3, B3, C3, D3) represents corresponding OCT B-Scans. The segmented superficial and deep layers in OCT B-Scans are marked in A3 and B3 respectively. Scale bar shown in A1 corresponds to 1.5 mm and applies to all the images.

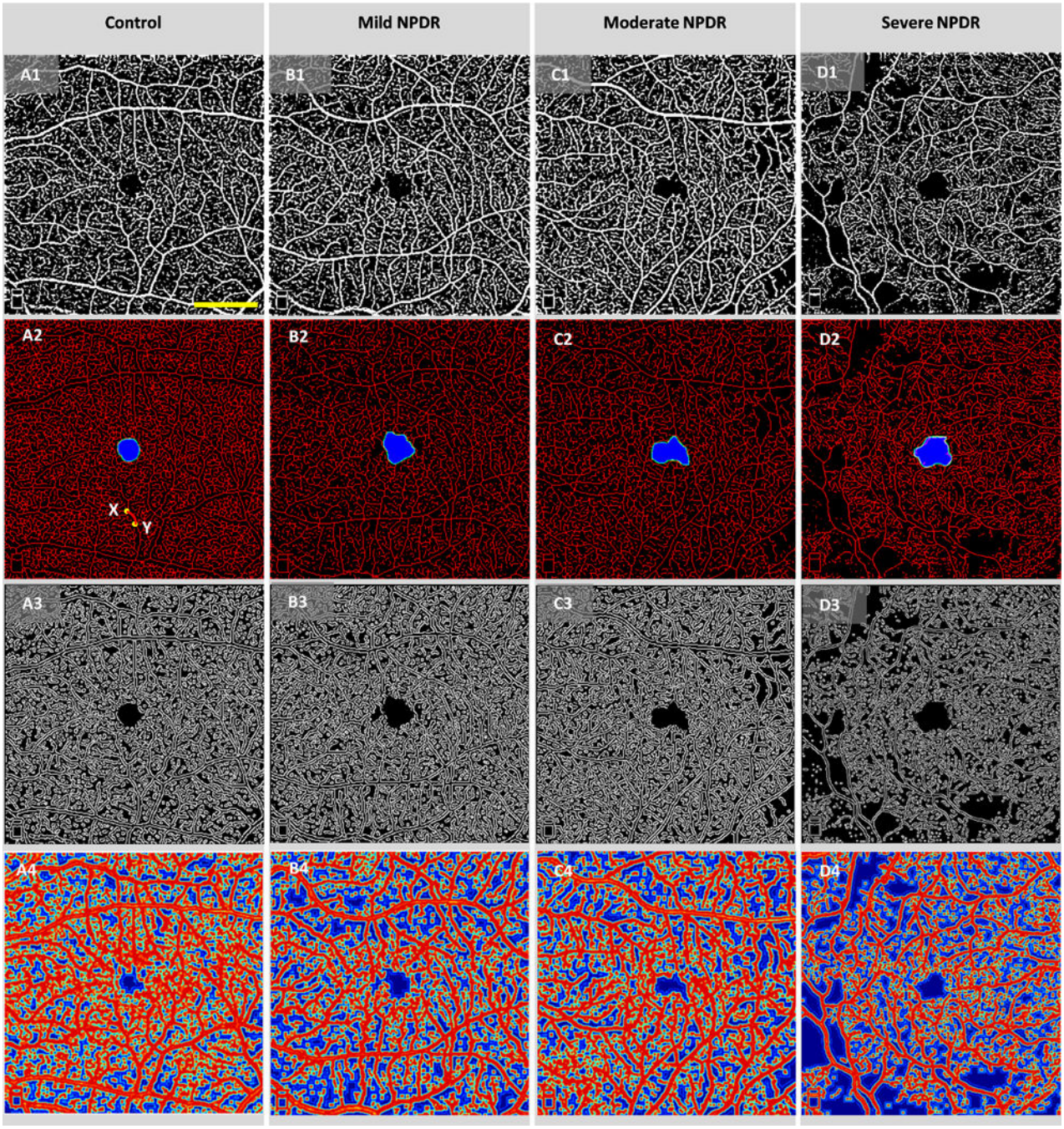

Figure 3.

Representative OCTA images for illustrating the feature extraction. (A1-A4) Control subject, (B1-B4) Mild NPDR subject, (C1-C4) Moderate NPDR subject, (D1-D4) Severe NPDR subject. (A1, B1, C1, D1) Segmented blood vessel map including large blood vessels and small capillaries. Hessian based Frangi vesselness filter and FD classification provide a robust and accurate blood vessel map. (A2, B2, C2, D2) Skeletonized blood vessel map (red) with segmented FAZ (marked blue region) and FAZ contour (green boundary marked around FAZ). A random vessel branch is highlighted in bright red (A2) with X and Y endpoints

identified in yellow dot. (A3, B3, C3, D3) Vessel perimeter map. (A4, B4, C4, D4) Contour maps created with normalized values of local fractal dimension. Scale bar shown in A1 corresponds to 1.5 mm and applies to all the images.

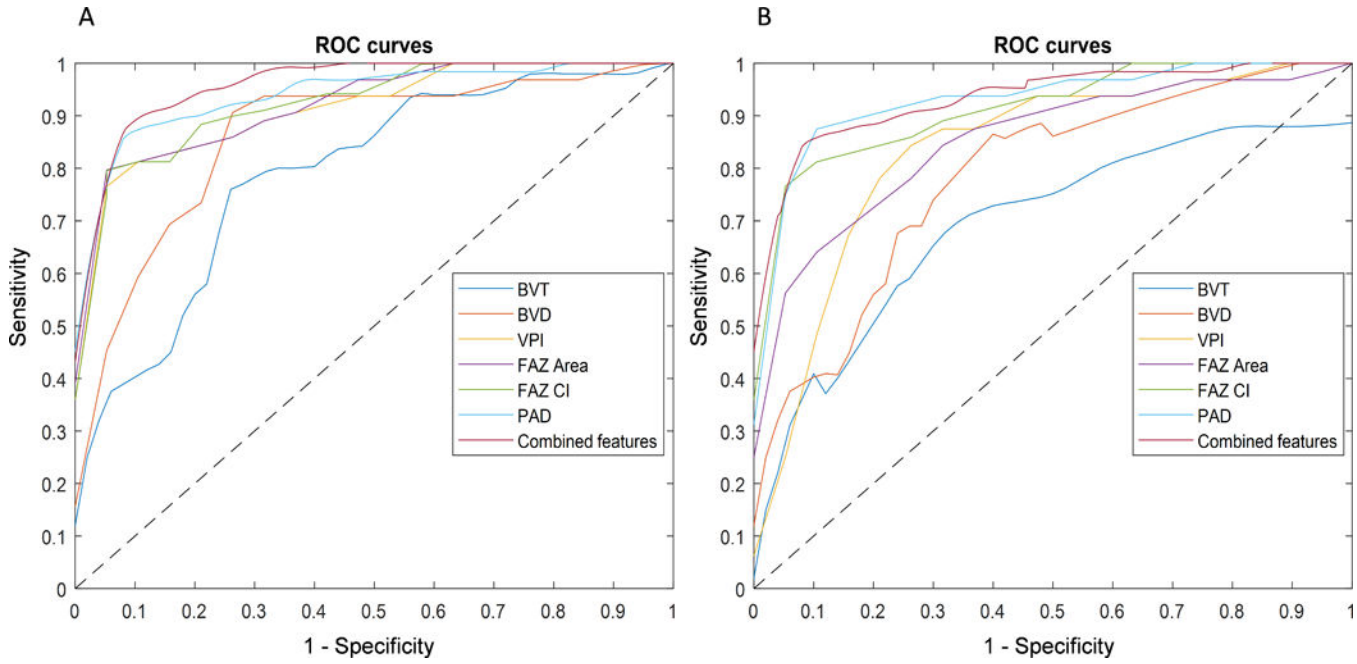

Figure 4.

The comparison of mean ROC curves for single and combined-features. (A) Control vs disease, (B) Control vs. mild NPDR. The dashed line represents the trade-off resulting from random chance.

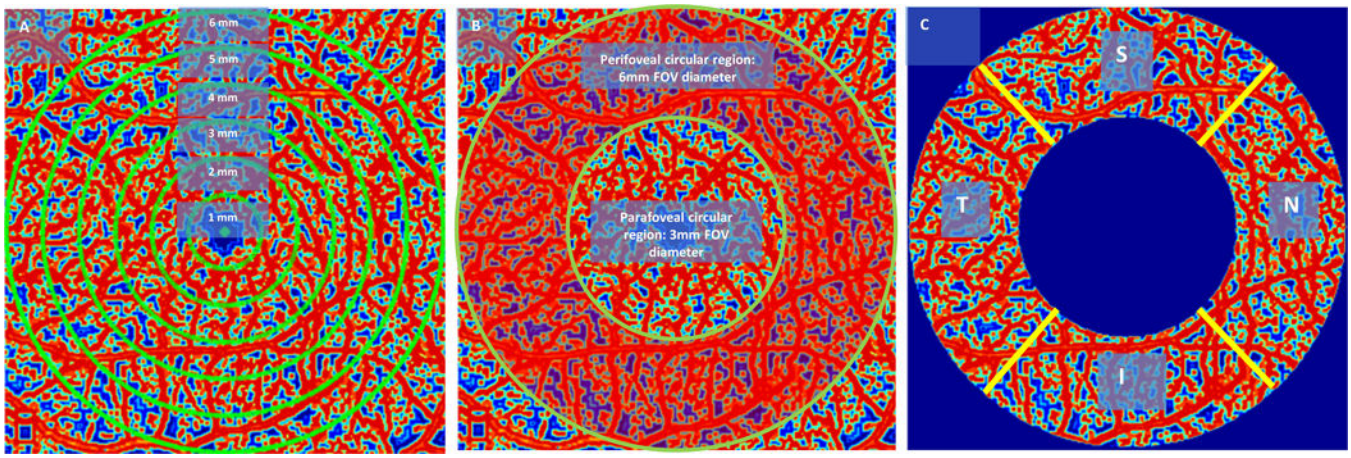

Figure 5.

Local fractal dimension contour maps with marked localized areas. (A) Circular regions with diameter 1–6 mm. (B) Most sensitive circular region. Circular region with diameter less than 3 mm is defined as parafoveal circular region. Circular region with diameter higher than 3 mm and lower than 6 mm is defined as perifoveal circular region. (C) Nasal, Superior, Temporal and Inferior regions shown in the perifoveal circular region.

Table 1.

Demographics of control and DR subjects.

		Diabetic Retinopathy		
	Control	**Mild NPDR**	**Moderate NPDR**	**Severe NPDR**
Number of subjects	20	20	20	20
Sex (male)	12	11	12	11
Age (mean ± SD), years	42 ± 9.8	50.1 ± 12.61	50.8 ± 8.39	57.84 ± 10.37
Age, range, years	25–71	24–74	32–68	41–73
Duration of diabetes, (mean ± SD), years	-	19.64 ± 13.27	16.13 ± 10.58	23.40 ± 11.95
Diabetes Type (%, type II)	-	100	100	100
Insulin dependent (Y/N)	-	7/13	12/8	15/5
HbA1C, %	-	6. 5 ± 0.6	7.3 ± 0.9	7.8 ± 1.3
HTN prevalence, %	10	45	80	80

[a]DR, diabetic retinopathy, SD, standard deviation, HbA1C, Glycated hemoglobin, HTN, hypertension

Table 2.

Quantitative summary of OCTA features for different DR stages.

	Control	Mild NPDR	Moderate NPDR	Severe NPDR	P values
BVT					
Superficial	1.11 ± 0.05	1.12 ± 0.04	1.18 ± 0.05	1.21 ± 0.04	0.044 †
BVC (μm)					
Superficial	17.84 ± 0.09	18.37 ± 0.28	20.43 ± 0.17	21.24 ± 0.21	0.038 *
VPI					
Superficial	10.57 ± 0.22	9.79 ± 0.61	8.93 ± 0.09	7.84 ± 0.37	0.006 *
BVD (%)					
Superficial	48.16 ± 3.32	45.62 ± 2.11	40 ± 3.52	36.84 ± 2.45	0.001 *
Deep	49.72 ± 3.18	45.98 ± 3.09	41.78 ± 2.17	37.46 ± 3.16	0.001 *
FAZ-A (mm^2)					
Superficial	0.29 ± 0.16	0.31 ± 0.17	0.36 ± 0.18	0.40 ± 0.21	0..006 †
Deep	0.46 ± 0.17	0.47 ± 0.15	0.52 ± 0.11	0.58 ± 0.26	0.006 †
FAZ-CI					
Superficial	1.16 ± 0.04	1.23 ± 0.13	1.31 ± 0.12	1.42 ± 0.13	0.004 *
Deep	1.19 ± 0.06	1.24 ± 0.29	1.34 ± 0.09	1.45 ± 0.14	0.005 *

[a] All values are presented as mean ± SD.

[b] BVT = Blood vessel tortuosity, BVC = Blood vessel caliber, VPI = Vessel perimeter index, BVD = Blood vessel density, FAZ-A = Foveal avascular zone – area, FAZ-CI = FAZ contour irregularity, NPDR = Non proliferative diabetic retinopathy.

* One-way ANOVA

† Kruskal-Wallis

Table 3.

Performance comparison between single and combined-features.

Parameters	Control vs disease (NPDR)				Control vs. mild NPDR			
	Sensitivity (%)	Specificity (%)	Accuracy (%)	AUC (%)	Sensitivity (%)	Specificity (%)	Accuracy (%)	AUC (%)
BVT	81.05	80.36	80.63	78.92	78.82	72.93	75.87	71.33
BVC	82.78	80.91	81.29	80.48	82.36	80.68	80.03	79.92
VPI	89.64	88.10	89.78	86.78	89.51	86.18	86.25	86.11
BVD	94.06	93.73	93.89	91.87	93.62	91.69	92.75	90.89
FAZ-A	92.25	91.70	92.02	90.79	91.64	90.91	91.26	87.81
FAZ-CI	93.83	92.98	93.48	90.98	92.56	91.38	92.19	90.32
Combined-features	**95.17**	**93.88**	**94.41**	**92.33**	**94.45**	**92.29**	**92.96**	**91.98**

[a]NPDR = Non proliferative diabetic retinopathy, AUC = Area under the (ROC) curve, BVT = Blood vessel tortuosity, BVC = Blood vessel caliber, VPI = Vessel perimeter index, BVD = Blood vessel density, FAZ-A = Foveal avascular zone area, FAZ-CI = Foveal avascular zone contour irregularity.

Table 4.

Classification performance using BVD from circular localized areas.

Locations	Control vs disease (NPDR)	Control vs. mild NPDR
	Accuracy (%)	Accuracy (%)
Circle 1: diameter 1 mm	53.70	50.67
Circle 2: diameter 2mm	70.53	64.82
Circle 3: diameter 3 mm	79.58	75.09
Parafoveal area : diameter < 3 mm	**80.65**	**76.22**
Circle 4: diameter 4 mm	82.22	81.64
Circle 5: diameter 5 mm	87.18	84.25
Circle 6: diameter 6 mm	87.94	86.43
Perifoveal area : 3 mm < diameter < 6 mm	**90.77**	**89.64**

[a]NPDR = Non proliferative diabetic retinopathy, BVD = Blood vessel density.

Table 5.

Classification performance using BVD from different orientations inside perifoveal circular region.

Orientation in perifoveal area	Control vs disease (NPDR)	Control vs. mild NPDR
	Accuracy (%)	Accuracy (%)
Nasal	81.53	79.24
Superior	86.96	84.50
Temporal	**87.79**	**86.33**
Inferior	82.63	80.42

[a]NPDR = Non proliferative diabetic retinopathy, BVD = Blood vessel density.